



A numerical study on turbulent flow around a square cylinder with uniform injection or suction

Burhan Çuhadaroğlu

*Department of Mechanical Engineering, Karadeniz Technical University,
Trabzon, Turkey*

Received 5 November 2007
Revised 10 June 2008
Accepted 5 August 2008

Abstract

Purpose – This paper aims to predict the effects of uniform injection or suction through a porous square cylinder on the flow field and on some aerodynamic parameters.

Design/methodology/approach – The finite volume method has been used for solving the ensemble averaged Navier–Stokes equations for incompressible flow in conjunction with the k - ϵ turbulence model equations including the Kato and Launder modification.

Findings – The parameters taken into account are injection or suction velocity, position of injection and suction surface, drag and lift coefficients and Strouhal number. The numerical results show that increasing suction velocity decreases the drag coefficient for all the suction configurations considered in the present study, except that of suction through rear surface. The vortex-shedding motion gets weak by the suction application through top and bottom surfaces.

Research limitations/implications – The problem is restricted with a 2-D simple geometry such as square cylinder due to the limited computer capability. Further extensions of the present study could include the more complex configurations and some other aspects such as heat transfer between porous cylinder and main flow.

Practical implications – The injection or suction application through a porous bluff body can be used as an efficient drag and vortex control method in aerodynamics.

Originality/value – This paper describes an attempt to simulate numerically the flow around square cylinder with uniform injection and suction in a manner different from what is given in the literature.

Keywords Porous materials, Fluid dynamics, Fluid engineering, Turbulent flow

Paper type Research paper

1. Introduction

The drag control of a body and the control of heat transfer from a surface are of primary interest for the fluid–solid interaction system designers, because of their wide range of applications: vibration control, dynamic install, lift and drag control, reduction of acoustic phenomena, thermal protection of high-speed spacecrafts, enhancement of heat transfer in heat exchangers, etc. The methods of drag control involve the control of vortex shedding behind bluff body, which heats the cylinder to modify the local flow properties or the use of localized discrete steady or unsteady injection or suction to change the circulation around the bluff body or the pressure distribution along its surface. Most studies on wall thermal protection deal with the technique of film cooling or discrete injection through holes.

Injection or suction through a porous layer or porous plate, which is used to control the characteristics of boundary layers, is an important research area in the fields of computational and experimental fluid dynamics. Injection from a porous plate thickens the boundary layer, thereby decreasing surface skin friction and hence the drag. Suction is performed to delay or avoid the boundary layer separation and to prevent the transition to turbulence. Even though the magnitude of transpiration rate is relatively lower than that of the mainstream, it significantly changes surface skin friction as well



as turbulence quantities near the wall. The effects of transpiration that reduce drag and provide thermal protection depend on the parameters of transpiration through porous plate i.e. velocity and angle of transpiration, etc. Bellettre *et al.* (1999) observed that on a porous plate with increasing injection rate, the friction factor and heat transfer coefficient significantly decrease. The results of this study were compared with experimental measurements and validated. Schetz and Nerney (1977) experimentally investigated and found that with increasing rate of injection, the velocity and turbulence intensity in the turbulent boundary layer increased. Injection is also an effective tool to produce film cooling for high-speed systems, which are exposed to high temperatures (e.g. nozzle of spacecraft engines and turbine blades). Meinert *et al.* (2001) showed that transpiration of a foreign gas through a porous wall into a turbulent boundary layer has a strong influence on heat transfer between the wall and the main flow. Çuhadaroğlu (2004) numerically studied the effects of tangential transpiration on the characteristics of turbulent boundary layer and found that local friction coefficient and thermal boundary layer thickness are substantially influenced by the velocity and the angle of transpiration.

The results of some typical benchmark contributions had been enlightening for bluff body aerodynamics with injection. In addition, the correlations of a turbulent flow that are measured for simple flows need to be modeled for flows having complex geometry such as bluff body flows. Lyn *et al.* (1995) presented the results of the LDA measurements on near-wake flow ($Re = 21,400$) around a square cylinder. The measurements have become a standard test case for unsteady turbulent flow of this kind because in these measurements, triple decomposition, which is considered in the present study, was introduced for data reduction to obtain phase-averaged quantities. Bosch and Rodi (1998) studied the simulation of vortex shedding past a square cylinder with different turbulence models. They showed that the main quantities of engineering interest can be predicted reasonably well with $k-\epsilon$ type models.

A number of researchers studied the convection problem on a porous vertical plate with surface mass transfer. Gorla *et al.* (1997) showed that the momentum and thermal boundary layer thicknesses increase in the case of injection and decrease with increasing suction. Although many investigators studied the turbulent boundary layers on a porous plate with injection and the flows around a bluff body without injection, a few dwelt on the effects of injection through a bluff body on the aerodynamic parameters. Included among these were Hannemann and Oertel (1989) who numerically proved that a sufficient base bleed from a flat plate, following the well-known experimental result, reduces the strength of the vortex street for unsteady laminar flows. Schumm *et al.* (1994) also studied vortex-shedding control measures such as wake heating, transverse body oscillations and base bleed in laminar flow. Mathelin *et al.* (2002) numerically studied the flow around a porous circular cylinder in a cross-flow when complete blowing was applied. One result of this study revealed that the pressure defect at the rear of the circular cylinder tended to “fill up” with blowing, leading to lower transverse static pressure gradients in the near wake. Jue (2004) studied the vortex shedding behind a porous square cylinder for laminar flow and concluded that the Darcy number demonstrates more influence on the flow field than porosity does. Fransson *et al.* (2004) presented an experimental study on the flow around a porous cylinder subject to continuous suction or blowing. It was observed that the drag of cylinder increased linearly with the blowing rate, whereas for suction there was a drastic decrease at a specific rate.

In the present study, it is attempted to simulate numerically the flow around square cylinder with uniform injection and suction in a manner different from what is given in the literature. The modified k-ε model is treated as a RANS model, and its applicability in simulating the aerodynamic characteristics of square cylinder in smooth flow investigated. The parametric results of no-injection square cylinder have been compared with the data given in the literature and a good agreement has been obtained. The verified results of the no-injection and suction case have encouraged the study of the flow around square cylinder with uniform injection and suction.

2. Mathematical formulation

2.1. Governing equations

The present study is concerned with an unsteady flow around a bluff body, in which the turbulent fluctuations ϕ' are superimposed on the periodic unsteady motion $\langle\phi\rangle(t)$ of the vortex shedding in the wake of square cylinder. By this definition, the instantaneous flow quantities $\phi(t)$ are separated into a time mean component $\bar{\phi}$, a periodic component $\tilde{\phi}(t)$ and the turbulent fluctuating component ϕ' :

$$\phi(t) = \bar{\phi} + \tilde{\phi}(t) + \phi' = \langle\phi\rangle(t) + \phi' \tag{1}$$

The combination of the time mean and the periodic part is called the ensemble-averaged component $\langle\phi\rangle(t)$, which is considered in the present numerical analysis. In a numerical simulation of a flow with vortex shedding, due to the numerical restrictions, time step of discretization equations will take a lower value than that of the period of vortex. In other words, it should be considered that the ensemble-average process of the instantaneous flow quantities is limited by the time step of numerical scheme (Figure 1).

The continuity and the ensemble-averaged Navier–Stokes equations can be written as

$$\frac{\partial\langle u_j \rangle}{\partial x_j} = 0 \tag{2}$$

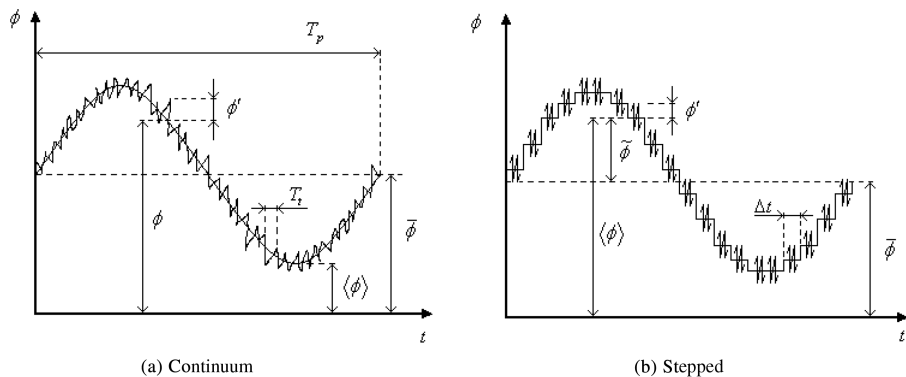


Figure 1.
Decomposition of a
turbulent unsteady
quantity

$$\frac{\partial \langle u_i \rangle}{\partial t} + \langle u_j \rangle \frac{\partial \langle u_i \rangle}{\partial x_j} = -\frac{1}{\rho} \frac{\partial \langle p \rangle}{\partial x_i} + \frac{\partial}{\partial x_j} \left[\nu \left(\frac{\partial \langle u_i \rangle}{\partial x_j} + \frac{\partial \langle u_j \rangle}{\partial x_i} \right) - \langle u_i' u_j' \rangle \right] \quad (3)$$

Here u_i is the local instantaneous velocity component in x_i direction, p is the instantaneous pressure, ν and ρ are the fluid kinematic viscosity and density. Within the framework of an eddy viscosity and adopting the Boussinesq approximation, the Reynolds stress is approximated as

$$-\langle u_i' u_j' \rangle = \langle \nu_t \rangle \left(\frac{\partial \langle u_i \rangle}{\partial x_j} + \frac{\partial \langle u_j \rangle}{\partial x_i} \right) - \frac{2}{3} \delta_{ij} \langle k \rangle \quad (4)$$

This concept works on the assumption that the Reynolds stresses are proportional to the local ensemble-averaged velocity gradients and that the proportionality factor, the eddy viscosity, ν_t , is a scalar quantity. In the present study, the RANS model is used in a 2-D high Reynolds number flow. This is based upon the hypothesis that if the spanwise turbulent fluctuation is supposed to be homogeneous, the spatial average of its fluctuation in the direction of the span is equivalent to its ensemble average. Based on this hypothesis, Franke and Rodi (1991) showed that for a square cylinder in a smooth flow its Strouhal number and mean drag coefficient are reproduced well by the unsteady 2-D analysis using the Reynolds-stress equation model in conjunction with a wall function (WF). They also showed that the using of the conventional standard k - ϵ model with the WFs in an unsteady 2-D analysis, vortex shedding can not be simulated, and even with a two-layer (TL) model the periodic vortex shedding is weak. Kato and Launder (1993) used the property of irrotationality of the flow at the upstream region to remove this defect and proposed a modification to the k - ϵ model in which production of turbulent kinetic energy is expressed in terms of a vorticity tensor and a velocity strain tensor. The model equations are:

$$\frac{\partial \langle k \rangle}{\partial t} + \langle u_j \rangle \frac{\partial \langle k \rangle}{\partial x_j} = \frac{\partial}{\partial x_j} \left[\left(\nu + \frac{\langle \nu_t \rangle}{\sigma_k} \right) \frac{\partial \langle k \rangle}{\partial x_j} \right] + P_k - \langle \epsilon \rangle \quad (5)$$

$$\frac{\partial \langle \epsilon \rangle}{\partial t} + \langle u_j \rangle \frac{\partial \langle \epsilon \rangle}{\partial x_j} = \frac{\partial}{\partial x_j} \left[\left(\nu + \frac{\langle \nu_t \rangle}{\sigma_\epsilon} \right) \frac{\partial \langle \epsilon \rangle}{\partial x_j} \right] + C_1 P_k \frac{\langle \epsilon \rangle}{\langle k \rangle} - C_2 \frac{\langle \epsilon \rangle^2}{\langle k \rangle} \quad (6)$$

$$\langle \nu_t \rangle = C_\mu \langle k \rangle^2 / \langle \epsilon \rangle \quad (7)$$

With the modification of Kato and Launder (1993) for the production of $\langle k \rangle$:

$$P_k = C_\mu \langle \epsilon \rangle S \Omega, \quad S = \frac{\langle k \rangle}{\langle \epsilon \rangle} \sqrt{\frac{1}{2} \left[\frac{\partial \langle u_i \rangle}{\partial x_j} + \frac{\partial \langle u_j \rangle}{\partial x_i} \right]^2}$$

$$\text{and} \quad \Omega = \frac{\langle k \rangle}{\langle \epsilon \rangle} \sqrt{\frac{1}{2} \left[\frac{\partial \langle u_i \rangle}{\partial x_j} - \frac{\partial \langle u_j \rangle}{\partial x_i} \right]^2}$$

Where S is the symmetric deformation of the fluid, while Ω is a rotation parameter and

is proportional to the magnitude of the local vorticity. The values of the $k-\varepsilon$ model constants are: $\sigma_k = 1.0, \sigma_\varepsilon = 1.3, C_1 = 1.44, C_2 = 1.92$ and $C_\mu = 0.09$. The modification of Kato and Launder (KL) is suitable for general flow configurations involving stagnation regions, not only for vortex-shedding flows.

2.2 Boundary conditions

The inlet of the computational domain is located at $x/H = -4.5$ (the coordinate system has its origin in the centre of the front surface of the cylinder). At this boundary, conditions are specified with constant values for the velocities and the turbulence quantities (Figure 2):

$$\langle \vec{u} \rangle = (u_\infty, 0), \langle k \rangle = 1.5(Tu \cdot u_\infty)^2, \langle \varepsilon \rangle = C_\mu \langle k \rangle^2 / \nu_{t-in} \tag{8}$$

where Tu is the turbulence intensity at the inlet and considered as 2 percent in the present computations. The dissipation rate $\langle \varepsilon \rangle$ at the inflow boundary is computed from (7) by specifying the ratio $r_\mu = \nu_{t-in} / \nu$. The commonly accepted value of r_μ is about 100 has been choose in the present calculations (Bosch and Rodi, 1998). The inlet conditions are also used as initial conditions on the computational domain.

Along the free boundaries, where the flow field is considered fully developed, the gradients normal to the boundary and normal velocity vanish as:

$$\frac{\partial \langle \phi \rangle}{\partial y} = 0, \langle v \rangle = 0 \tag{9}$$

At the outlet computation domain, which placed at $x/H = 25.5$ downstream of the cylinder, a zero streamwise gradient is specified as:

$$\frac{\partial \langle \phi \rangle}{\partial x} = 0 \tag{10}$$

In the near-porous wall region, which has two sub-layers, two different formulas have been used in computational algorithm. Regarding y -direction as normal direction, the viscous sub-layer was simulated as

$$\langle u^+ \rangle = \frac{\exp(\langle y^+ \rangle \langle v_w^+ \rangle) - 1}{\langle v_w^+ \rangle} \tag{11}$$

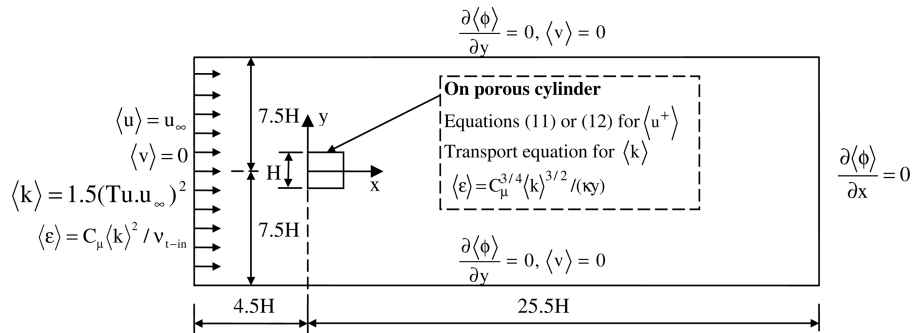


Figure 2. Boundary conditions

and in the log-law layer

$$\langle u^+ \rangle = \left\{ \frac{\langle v_w^+ \rangle}{4\kappa} \ln \left| \frac{\langle y^+ \rangle}{y_p^+} \right| + \left(1 + u_p^+ \langle v_w^+ \rangle \right)^{1/2} \right\} \frac{1}{\kappa} \ln \left| \frac{\langle y^+ \rangle}{y_p^+} \right| + u_p^+ \quad (12)$$

has been regarded with the constants of $u_p^+ = y_p^+ = 11.5$ and $\kappa = 0.4$ (Çuhadaroğlu, 2004). Finally, the WFs used in this study can be summarized as follows:

$$\langle u^+ \rangle = \begin{cases} \text{Equation (11);} & \text{for } \langle y^+ \rangle < y_p^+ \\ \text{Equation (12);} & \text{for } \langle y^+ \rangle \geq y_p^+ \end{cases} \quad (13)$$

Near the wall, the log-law region is in local equilibrium so that the rate of turbulence kinetic energy production is approximately equal to its dissipation rate. Therefore, at the point close to the porous wall, the value of turbulence kinetic energy $\langle k \rangle$ is calculated by solving the transport equation of turbulence kinetic energy, while the energy dissipation $\langle \varepsilon \rangle$ can be evaluated by the expression

$$\langle \varepsilon \rangle = \frac{C_\mu^{3/4} \langle k \rangle^{3/2}}{\kappa y} \quad (14)$$

which was obtained from the transport equation of $\langle k \rangle$ by equating the production term to dissipation term.

3. Computational method

3.1 Method of solution

The governing equations were solved using the finite volume method in which the discretization equations were derived by integrating the differential equations over a defined control volume. Gauss's divergence theorem was used to relate the volume integrals to surface integrals. The calculation domain was discretized, as is generally done, with a staggered grid that allows prediction of the velocity components in the momentum grid points with the QUICK scheme, while the other variables, such as turbulence, kinetic energy and dissipation were predicted in the basic grid points with the HYBRID scheme. The method of numerical solution used in the present study is based on solving the set of discretization equations iteratively using Gauss–Seidel method with dimensionless time step of $\Delta t^* = 0.001$ ($\Delta t^* = \Delta t \cdot u_\infty / H$). At each new time step, after iterative solution, following Marker and Cell method (Hirt and Cook, 1972), the pressure was computed and the velocity components were corrected satisfying the continuity equation until the pressure difference at each grid point fell below 10^{-4} . The iterative solution of the discretization equations was continued until such time that periodic motion was obtained ($t^* = 200$). All computations were performed on a PC.

3.2 Computational domain and grid generation

The grid cells of computational domain were divided into three parts with a prescribed ratio of priority. The domain of the front of cylinder has 25 percent of the total grid cells on x-direction, while the top–bottom domains of cylinder have 25 percent and the rear of cylinder has 50 percent. Top–bottom domains of cylinder have 30 percent of the total grid cells on y-direction, while front–rear domains have 40 percent. The grid spacing

was arranged in non-uniform pattern with high-density grid points around the cylinder according to the grid expansion implicit formulae $r_{\text{exp}} = \left[\frac{x_L / (\Delta x_i)_{\text{min}}}{(r - 1) + 1} \right]^{1/\text{cell-num}}$, where x_L is the length of the sub-domain, “cell-num” is number of cells of the sub domain on grid expansion direction and $(\Delta x_i)_{\text{min}}$ is the width of the first cells adjacent to the cylinder. In order to determine the numerical uncertainty, the computations for the flow around non-porous and porous square cylinder were performed on three geometrical similar grid sets of 128×80 , 96×60 and 72×46 . The grid expansion ratios were kept constant for the all grid sets as $r_{\text{exp}} = 1.0856$ in the front of the cylinder, 1.0054 along the sides and 1.0641 in the rear of the cylinder in the x-direction. In the y-direction, the grid is symmetric with respect to $y = 0$ and the expansion ratio $r_{\text{exp}} = 1.1657$ in the top-bottom of the cylinder and 1.0054 along the sides of the cylinder (Figure 3).

After obtaining a converged solution for each grid, the numerical uncertainties of computational results are quantified by using the grid convergence index (GCI) which is based on Richardson’s extrapolation theory (Roache, 1997; Cadafalch *et al.*, 2002). The procedure of the method is given below. For a quantity ϕ obtained from three different grid sets, the apparent order p is calculated using the expression

$$r = \frac{1}{\ln(r_{21})} |\ln|\epsilon_{32}/\epsilon_{21}|q(p)| \quad (15.a)$$

$$q(p) = \ln \left[\frac{r_{21}^p - s}{r_{32}^p - s} \right] \quad (15.b)$$

$$s = 1.\text{sign}(\epsilon_{32}/\epsilon_{21}) \quad (15.c)$$

where r is the grid refinement factor as $r = h_{\text{coarse}}/h_{\text{fine}}$, h is the representative grid size as $h = \left[\sum_{i=1}^N (\Delta A_i) / N \right]^{1/2}$, ΔA_i is the area of the i th cell, N is the total number of cells used for computations, $\epsilon_{32} = \phi_3 - \phi_2$, $\epsilon_{21} = \phi_2 - \phi_1$, ϕ_k denoting the solution on the k th grid. The extrapolated values of ϕ :

$$\phi_{\text{ext}}^{21} = (r_{21}^p \phi_1 - \phi_2) / (r_{21}^p - 1) \quad (16.a)$$

$$\phi_{\text{ext}}^{32} = (r_{32}^p \phi_2 - \phi_3) / (r_{32}^p - 1) \quad (16.b)$$

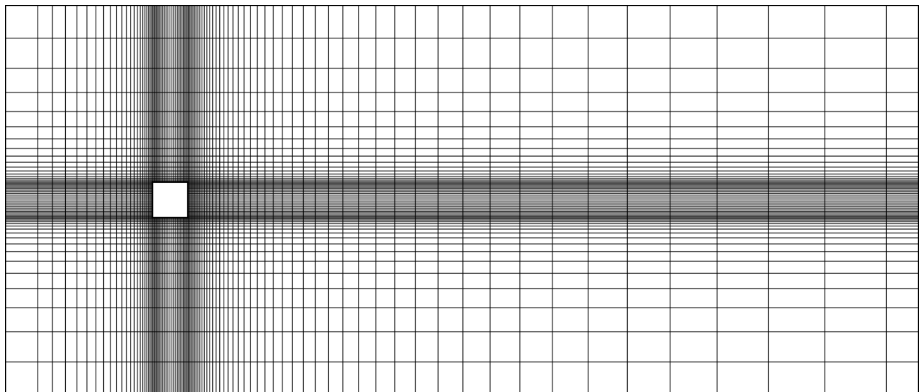


Figure 3.
Numerical grid (96 × 60)

The approximate relative errors:

$$e_a^{21} = \left| \frac{\phi_1 - \phi_2}{\phi_1} \right| \quad (17.a)$$

$$e_a^{32} = \left| \frac{\phi_2 - \phi_3}{\phi_2} \right| \quad (17.b)$$

The extrapolated relative errors:

$$e_{ext}^{21} = \left| \frac{\phi_{ext}^{12} - \phi_k}{\phi_{ext}^{12}} \right| \quad (18)$$

and the grid convergence indexes:

$$GCI^{21} = \frac{F_s e_a^{21}}{r_{21}^p - 1} \quad (19.a)$$

$$GCI^{32} = \frac{F_s e_a^{32}}{r_{32}^p - 1} \quad (19.b)$$

where a conservative value of $F_s = 1.25$ is recommended for three or more grid studies (Roache, 1997). The GCI reported in this study is the correction for grid solution of 96×60 . Numerical uncertainty of mean drag coefficient is represented by GCI values. Table I summarizes the numerical uncertainty of the time mean drag coefficient $\overline{C_D}$ for three selected grids in the case of no injection. As seen in Table I, numerical uncertainty improved from 5.4 percent between 72×46 and 96×60 grids to 1.25 percent between 96×60 and 128×80 grids.

Table II shows the GCI results of mean drag coefficients for the injection through all surfaces with $v_w = 0.002$ m/s. The uncertainty of the $\overline{C_D}$ is also improved from 30.8 to 18.3 percent with refinement from coarsest to finer grid for the injection through all surfaces. The GCI shows high numerical uncertainty due to the effect of injection on the velocity gradients around the cylinder. The widths of the minimum grids adjacent to the cylinder, which possess the major effect on the velocity gradients, decrease with refinement from coarsest to finest grid. In this study, 96×60 grid arrangement with

i	1	2	3
Grid	128 × 80	96 × 60	72 × 46
N	10,240	5,760	3,312
h	0.02096	0.02795	0.03686
$r = h_{i+1}/h_i$		1.33	1.32
$\phi(\overline{C_D})$	2.2026	2.1329	1.8558
$ \phi_{i+1} - \phi_i $		0.0697	0.2771
p		5.015	
ϕ_{ext}		2.2245	2.2245
e_a (%)		3.17	13
e_{ext} (%)	0.98	4.1	16.6
GCI (%)		1.25	5.4

Table I.
GCI for no injection

HF 19,6	i	1	2	3
	Grid	128 × 80	96 × 60	72 × 46
	N	10,240	5,760	3,312
	h	0.02096	0.02795	0.03686
	$r = h_{i+1}/h_i$	1.33		1.32
	$\phi(\overline{C_D})$	2.3849	2.1962	1.9155
	$ \phi_{i+1} - \phi_i $	0.1887		0.2807
	p		1.508	
	ϕ_{ext}	2.736		2.736
	e_a (%)	7.9		12.8
	e_{ext} (%)	12.8	19.7	30
	GCI (%)	18.3		30.8

716

Table II.
GCI for injection
through all surfaces with
 $v_w = 0.002$ m/s

the widths of the minimum grids as 0.00624, 0.00404 and 0.00838 m in front, top-bottom and rear surfaces, respectively, on x-direction has been considered, while as 0.00784, 0.00404 and 0.00784 m in bottom, front-rear and top surfaces respectively on y-direction, whereas the injection or suction velocities were varied.

4. Results and discussion

The $\overline{C_D}$ values of sharp-edged bodies, which tend to cause flow separation regardless of boundary layer, are independent of Re at $Re \geq 10^4$ (White, 1999). The relation between pressure coefficients of front-rear surfaces and the $\overline{C_D}$ can be expressed as

$$\overline{C_D} = \left(\int_{\text{front}} \overline{C_P} ds - \int_{\text{rear}} \overline{C_P} ds \right) / H - \left(\int_{\text{top}} \tau ds + \int_{\text{bottom}} \tau ds \right) / (\rho u_{\infty}^2 H / 2) \quad (20)$$

Similarly, the lift coefficient $\overline{C_L}$ has been determined by

$$\overline{C_L} = \left(\int_{\text{bottom}} \overline{C_P} ds - \int_{\text{top}} \overline{C_P} ds \right) / H - \left(\int_{\text{front}} \tau ds + \int_{\text{rear}} \tau ds \right) / (\rho u_{\infty}^2 H / 2) \quad (21)$$

where s is the line on the surfaces of the cylinder. The integrals of (20) and (21) have been calculated numerically based on the numerical data. The r.m.s. values of the drag and lift coefficients, which give an idea about vibration intensity, have been calculated by the time histories of the coefficients. The Strouhal numbers of the flows have been determined from the FFT analysis of the time history of the horizontal velocity component at the point of $x/H = 1.5$ and $y/H = 0$ located downstream of the cylinder.

An overall comparison of the numerical results of a non-porous square cylinder obtained for both WF and TL approach with KL modification with experiments have been given by Bosch and Rodi (1998). The results of the present study for flow around a non-porous square cylinder, which have been compared to the experimental results given by Lyn *et al.* (1995) and Durao *et al.* in Bosch and Rodi (1998), have been regarded as reference data to analyze the effects of injection or suction through a square cylinder on the flow field. Figure 4 shows the distribution of the non-dimensional time mean velocity component \bar{u}/u_{∞} on the cylinder centre-line at $y = 0$. As seen in Figure 4,

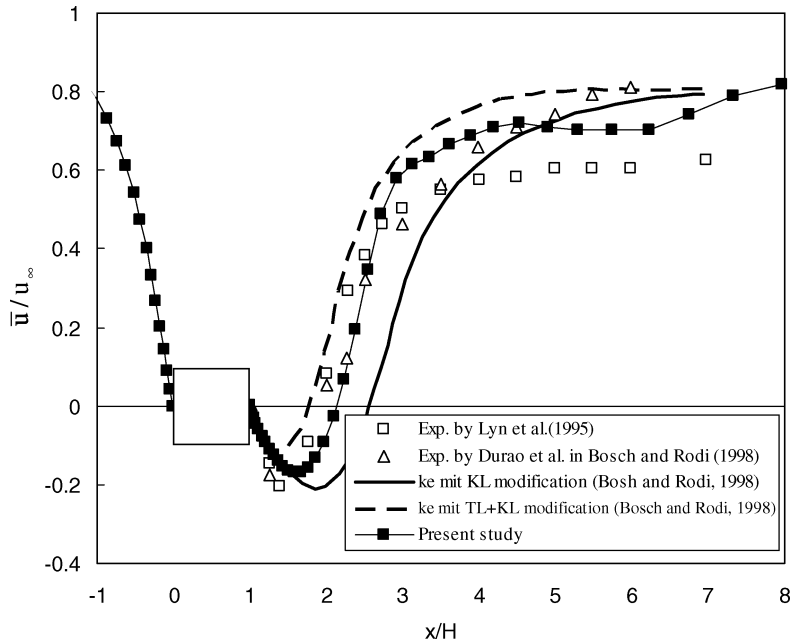


Figure 4.
 \bar{u}/u_∞ on the centre-line of
the cylinder without
injection

although the length of the recirculation zone of the present study approach the experimental values, the \bar{u}/u_∞ values dissimilar the experiments of Lyn *et al.* (1995) ahead of the recirculation zone for the no-injection flow.

In Figure 5, the distribution of the non-dimensional time mean turbulent kinetic energy \bar{k}/u_∞^2 on the centre-line is shown obtained with no-injection data given in the literature. In this plot, the measured distribution of Lyn *et al.* (1995) and the calculation results of Bosch and Rodi (1998) using the standard $k-\epsilon$ model KL modification with and without a TL approach are shown. All the calculations can be seen to lie considerably below the experimental results. The no-injection \bar{k}/u_∞^2 results of the present study show good agreement with the calculation results of Bosch and Rodi (1998) using the standard $k-\epsilon$ model with KL modification and without a TL approach.

The porous square cylinder, which is convenient for injection or suction through plane surface(s), differs from porous circular cylinder. Each position of injection or suction surface influences the flow and aerodynamic parameters. In the present study, some representative configurations of the porous surfaces of square cylinder have been considered for analyzing the problem. The injection and suction velocity is expressed through the parameter $\Gamma = (v_w/u_\infty) \times 100$, where v_w is the velocity through the porous cylinder, positive for injection and negative for suction, and u_∞ is the oncoming streamwise velocity. The range of Γ investigated in the present study is $-10 < \Gamma < 6$.

4.1 Injection or suction through front surface

According to the parametric results of injection or suction through front surface, the \bar{C}_D increased with increasing injection velocity and decreased with increasing suction velocity (Table III). Obviously, this is the result of increasing pressure difference between front and rear surfaces by injection through front surface (opposite to the main flow) and vice versa for suction. Stated another way, the injection or suction

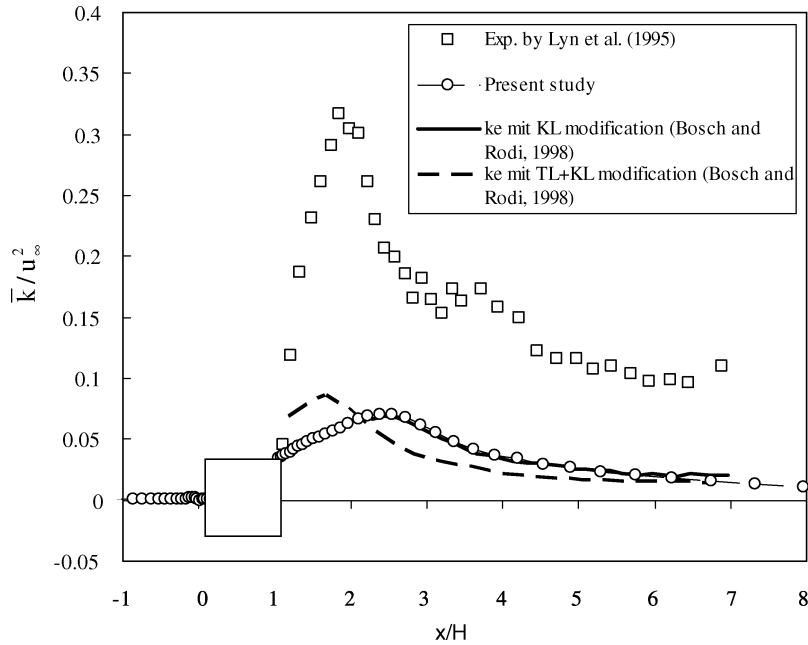


Figure 5.
 \bar{k}/u_∞^2 on the centre-line of the cylinder without injection

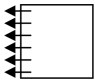
Configuration	Application	Γ	\bar{C}_D	C'_D	\bar{C}_L	C'_L	St
	Injection	6	2.1876	0.0414	0.0087	1.4021	0.1343
		5	2.1763	0.0412	0.0234	1.3913	0.1343
		4	2.1658	0.0411	0.0342	1.3873	0.1343
		3	2.1557	0.0412	0.0420	1.3880	0.1343
		2	2.1449	0.0421	0.0388	1.3872	0.1343
		1	2.1321	0.0447	0.0247	1.3849	0.1343
	No injection	0	2.1154	0.0470	0.0054	1.3837	0.1343
	Suction	-1	2.0990	0.0489	-0.0044	1.3945	0.1343
		-2	2.0831	0.0492	0.0042	1.3816	0.1343
		-3	2.0650	0.0491	-0.0041	1.3666	0.1343
-4		2.0479	0.0497	-0.0142	1.3540	0.1343	
-5		2.0266	0.0506	-0.0220	1.3441	0.1343	
-6		2.0091	0.0519	-0.0230	1.3424	0.1221	
-7		1.9870	0.0541	-0.0256	1.3299	0.1221	
-8		1.9712	0.0561	-0.0025	1.3228	0.1221	
-9		1.9538	0.0590	0.0155	1.3062	0.1221	
-10		1.9344	0.0658	0.0229	1.2980	0.1221	

Table III.
Results for injection or suction through front surface

through the front surface influence the \bar{C}_D principally by way of pressure difference increment or decrease between the front and rear surfaces.

The relation of the r.m.s. values of C_D with injection or suction velocity reveals that increasing injection velocity slightly decreases the C'_D , while the increasing suction velocity increases the C'_D . In the case of injection or suction through any surface, the variations of \bar{C}_L and C'_L with injection and suction velocity have no physical effect, except when the injection and suction are through top surface which cause an asymmetrical flow.

The values of the St number reveal that the St is not influenced by the injection and tends to decrease with increasing suction velocity through front surface. In other words, suction application through front surface for the higher values of the Γ decreases the frequency of vortex shedding in the wake (Table III).

The distributions of the non-dimensional time mean velocity component \bar{u}/u_∞ and the time mean turbulent kinetic energy \bar{k}/u_∞^2 on the cylinder centre-line at $y = 0$ show that the injection or suction through front surface have no effect on the wake flow (Figures 6 and 7).

4.2 Injection or suction through top surface

In the case of injection or suction through top surface, the relation of $\overline{C_D}$ with Γ follows the same trend as that of injection and suction through front surface. The C'_D values of this configuration indicate that increasing suction velocity increases the fluctuation of $\overline{C_D}$ substantially, while increasing injection velocity increases it only slightly. The injection or suction through top surface significantly affected the C_L as expected (Table IV). The suction through top surface contributes to lift on square cylinder, while injection affects the lift negatively.

The St number is impressively influenced by suction through top surface, in which the unsteady flow field around no injection and suction square cylinder tends to become steady with increasing suction through top surface. In contrast, increasing injection through top surface decreases the periodicity of the wake flow (Table IV). As seen in Figures 8 and 9, the injection or suction through top surface has no discernible effect on the wake flow.

4.3 Injection or suction through rear surface

Increasing the injection velocity through rear surface decreases the $\overline{C_D}$, while increasing suction velocity drastically increases the $\overline{C_D}$ as seen in Table V. The increasing suction

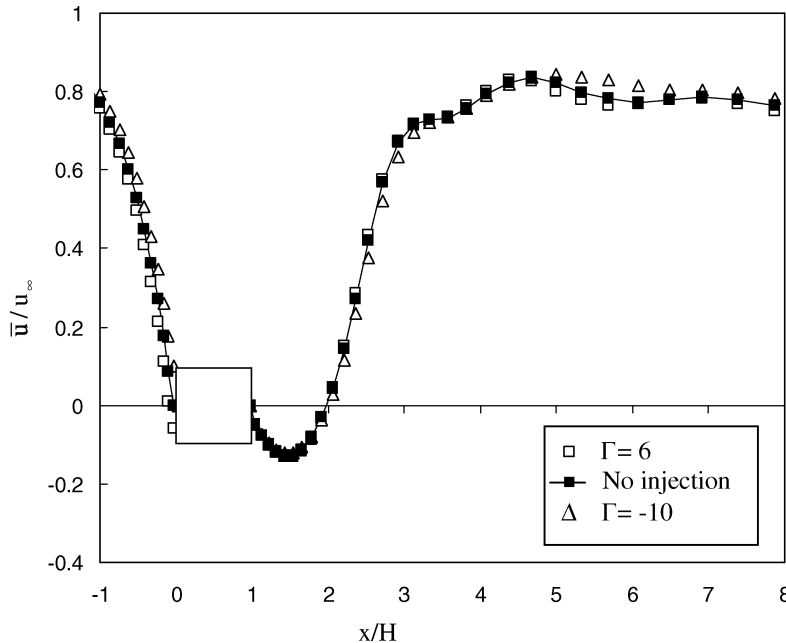


Figure 6.
 \bar{u}/u_∞ on the centre-line of the cylinder for the injection or suction through front surface

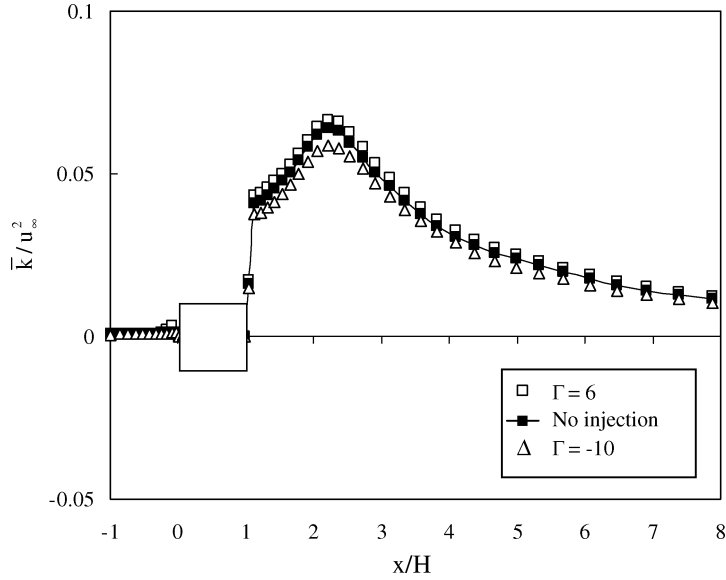


Figure 7.
 \bar{k}/u_∞^2 on the centre-line of the cylinder for the injection or suction through front surface

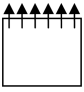
Configuration	Application	Γ	\bar{C}_D	C'_D	\bar{C}_L	C'_L	St	
	Injection	6	2.2528	0.0547	-0.4889	1.0678	0.1465	
		5	2.2298	0.0478	-0.4290	1.0851	0.1465	
		4	2.2031	0.0395	-0.3289	1.1095	0.1465	
		3	2.1716	0.0316	-0.2771	1.1298	0.1343	
		2	2.1405	0.0271	-0.1899	1.1786	0.1343	
	No injection	1	2.1197	0.0313	-0.1123	1.2536	0.1343	
		0	2.1154	0.0470	0.0054	1.3837	0.1343	
		Suction	-1	2.1142	0.0628	0.0975	1.4834	0.1343
			-2	2.1057	0.0695	0.3004	1.5249	0.1221
			-3	2.0900	0.0757	0.3839	1.5247	0.1221
-4	2.0949		0.1524	0.4871	1.4920	0.1099		
-5	2.0983		0.1817	0.7107	1.4167	0.1099		
	-6	2.1054	0.2475	1.0120	1.4140	0.0977		
	-7	2.1002	0.2840	1.1549	1.5321	0.0977		
	-8	2.0639	0.2732	1.2829	1.5354	0.0977		
	-9	2.0209	0.2675	1.4360	1.5584	0.0977		
	-10	2.0209	0.3171	1.5907	1.7287	0.0977		

Table IV.
Results for injection or suction through top surface

velocity through rear surface decreases the pressure on the rear surface of the cylinder and hence the pressure difference between front and rear surfaces increases which causes to increase the \bar{C}_D . The C'_D variation with Γ indicates that increasing injection velocity decreases the fluctuation of C_D , while increasing suction velocity increases the fluctuation of C_D . The St is not influenced by the injection or suction for the range of $6 \leq \Gamma \leq -5$, and takes the value of 0.1221 for the greater values of suction than $\Gamma = -6$ in the case of injection or suction through rear surface (Table V).

The distributions of the \bar{u}/u_∞ on the centre-line reveal that the increasing injection velocity through rear surface enlarges the recirculation zone and the recirculation zone

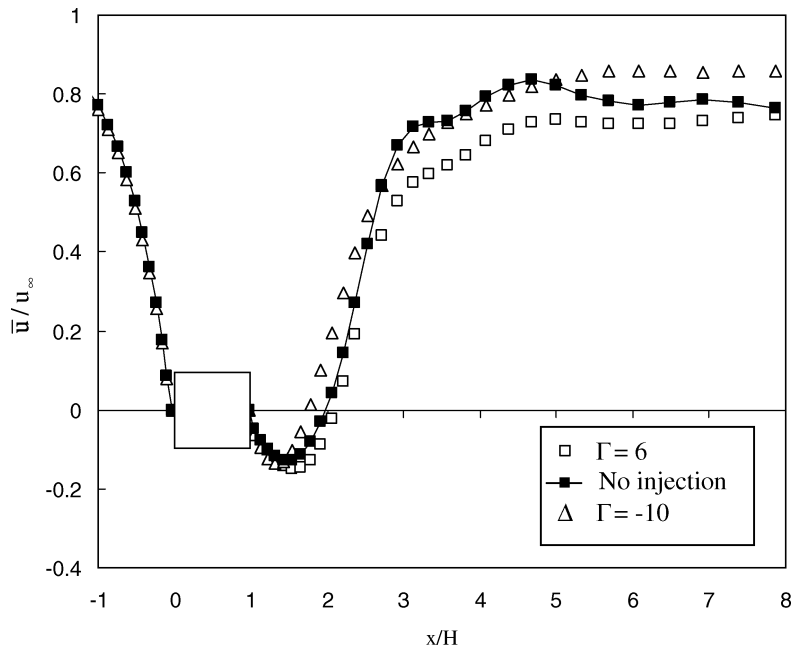


Figure 8.
 \bar{u}/u_∞ on the centre-line of
the cylinder for the
injection or suction
through top surface

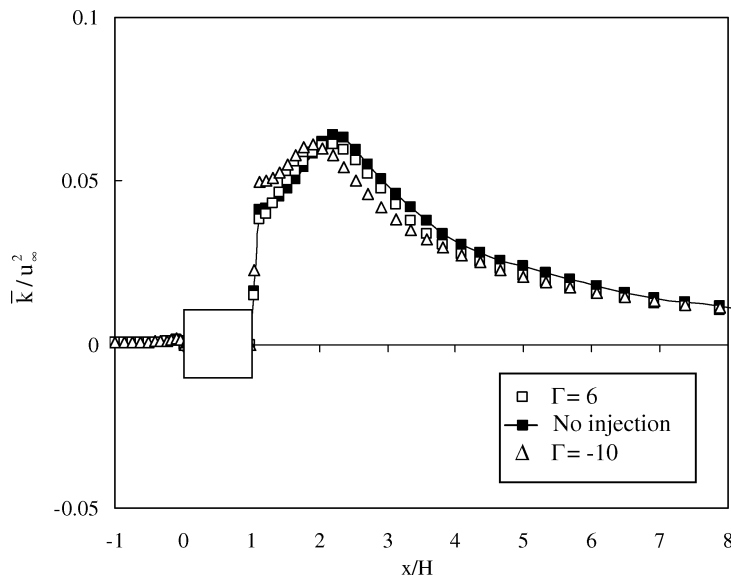


Figure 9.
 \bar{k}/u_∞^2 on the centre-line of
the cylinder for the
injection or suction
through top surface

shrinks until the suction value of $\Gamma = -4$. The higher values of the suction enlarge the recirculation zone again as seen in Figure 10. This trend reveals that the higher suction velocities than $\Gamma = -5$ through rear surface fairly bond the primary vortex formation to the cylinder and the separated flow from the rear corners of the cylinder creates a secondary vortex formation in the wake.

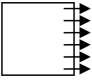
Configuration	Application	Γ	\bar{C}_D	C'_D	\bar{C}_L	C'_L	St
	Injection	6	2.0412	0.0357	-0.0307	1.0550	0.1343
		5	2.0454	0.0365	-0.0280	1.1090	0.1343
		4	2.0541	0.0385	-0.0210	1.1728	0.1343
		3	2.0652	0.0403	-0.0158	1.2333	0.1343
		2	2.0779	0.0445	-0.0111	1.3374	0.1343
	Suction	1	2.0941	0.0423	-0.0013	1.2902	0.1343
		0	2.1154	0.0470	0.0054	1.3837	0.1343
		-1	2.1414	0.0509	0.0223	1.4391	0.1343
		-2	2.1768	0.0575	0.0458	1.5053	0.1343
		-3	2.2271	0.0684	0.0653	1.5628	0.1343
	-4	2.3451	0.1016	0.0247	1.6401	0.1343	
	-5	4.9699	0.5063	-0.0526	2.2129	0.1343	
	-6	4.9202	0.5692	-0.0068	2.2490	0.1221	
	-7	4.8816	0.6216	0.0208	2.2415	0.1221	
	-8	4.8664	0.6578	-0.0493	2.2535	0.1221	
	-9	4.8556	0.6730	-0.1169	2.2531	0.1221	
	-10	4.8726	0.6688	-0.1498	2.2791	0.1221	

Table V.
Results for injection or suction through rear surface

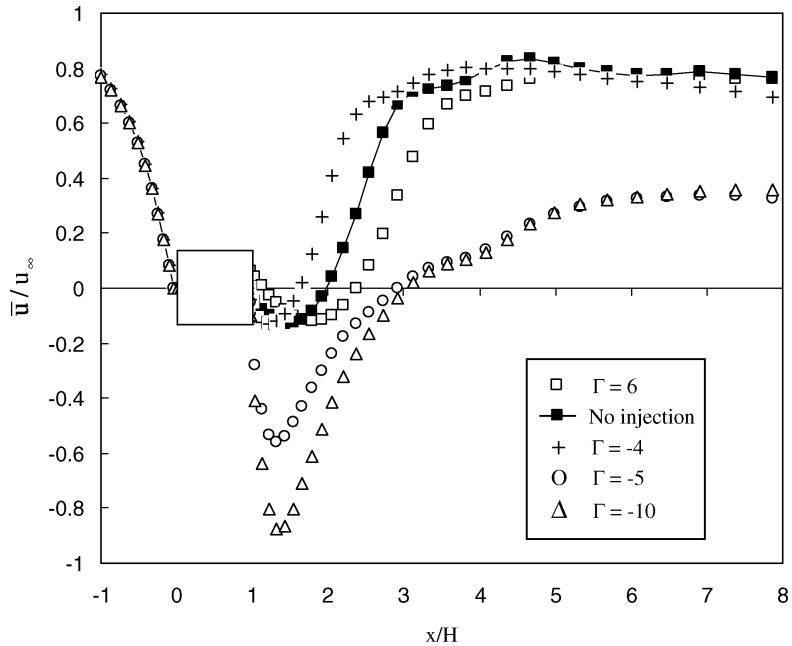


Figure 10.
 \bar{u}/u_∞ on the centre-line of the cylinder for the injection or suction through rear surface

The peak values of the \bar{k}/u_∞^2 distribution on the centre-line indicate the bounds of the vortex formations. As seen in Figure 11, the suction application through rear surface with $\Gamma = -5$ has two peak values of the \bar{k}/u_∞^2 at $x/H = 1.65$ and 4.37 which are the bounds of the primary and secondary vortex formations, respectively. Likewise, the suction through rear surface with $\Gamma = -10$ creates two different vortex formations which have the bounds at $x/H = 1.65$ and 4.99 (Figure 11).

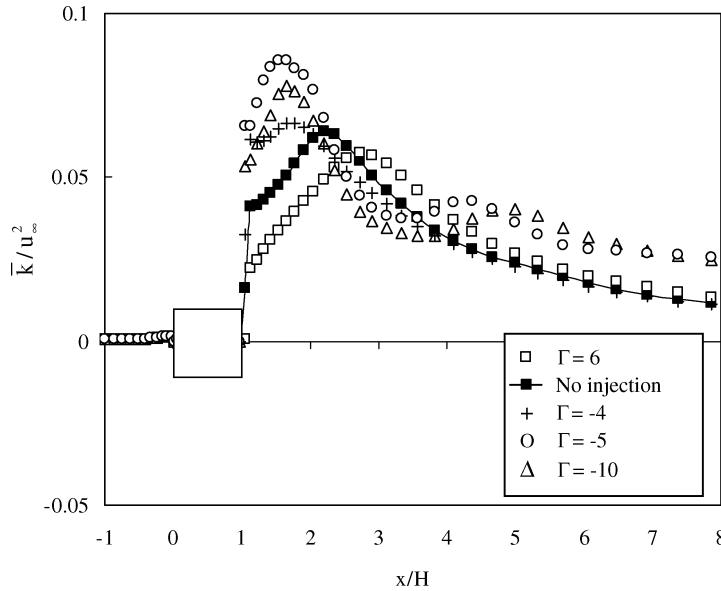


Figure 11.
 \bar{k}/u_∞^2 on the centre-line of the cylinder for the injection or suction through rear surface

4.4 Injection or suction through top and bottom surfaces

In this configuration, the \bar{C}_D has the lowest value for $\Gamma = -10$ compared to the other injection or suction applications as seen in Table VI. The results obtained for this configuration, in terms of aerodynamic parameters such as C_D and St , are the most striking. The injection through both top and bottom surfaces has “widen effect” on the flow field around square cylinder in vertical direction to result in increasing the \bar{C}_D , while suction through top and bottom surfaces “constricts” the flow field. The effect of the injection or suction through top and bottom surfaces on the \bar{C}_D show that the pressures on the rear surface decrease by the increasing injection through top and bottom surfaces and vice versa for the suction. The highest and lowest values of the St were obtained for the high injection velocities and high suction velocities, respectively, in this configuration.

Configuration	Application	Γ	\bar{C}_D	C'_D	\bar{C}_L	C'_L	St
	Injection	6	2.4885	0.0460	-0.0027	1.1466	0.1587
		5	2.4188	0.0370	0.0311	1.1269	0.1587
		4	2.3467	0.0283	-0.0200	1.1192	0.1465
		3	2.2621	0.0177	-0.0462	1.0849	0.1465
		2	2.1907	0.0157	-0.0230	1.0960	0.1465
		1	2.1427	0.0268	-0.0485	1.1983	0.1343
No injection	0	2.1154	0.0470	0.0054	1.3837	0.1343	
Suction	-1	2.1057	0.0757	0.0378	1.5907	0.1221	
	-2	2.0827	0.1037	0.0221	1.7133	0.1221	
	-3	2.0554	0.1479	0.0991	1.7061	0.1099	
	-4	2.0554	0.2761	0.0809	1.5698	0.1099	
	-5	2.0456	0.3196	0.0649	1.6265	0.0977	
	-10	1.7357	0.1774	0.0634	1.1317	0.0610	

Table VI.
Results for injection and suction through top and bottom surfaces

The distributions of the non-dimensional time mean velocity component on the cylinder centre-line show that the both injection and suction through top and bottom surfaces reduce the vortex formation length (Figures 12 and 13).

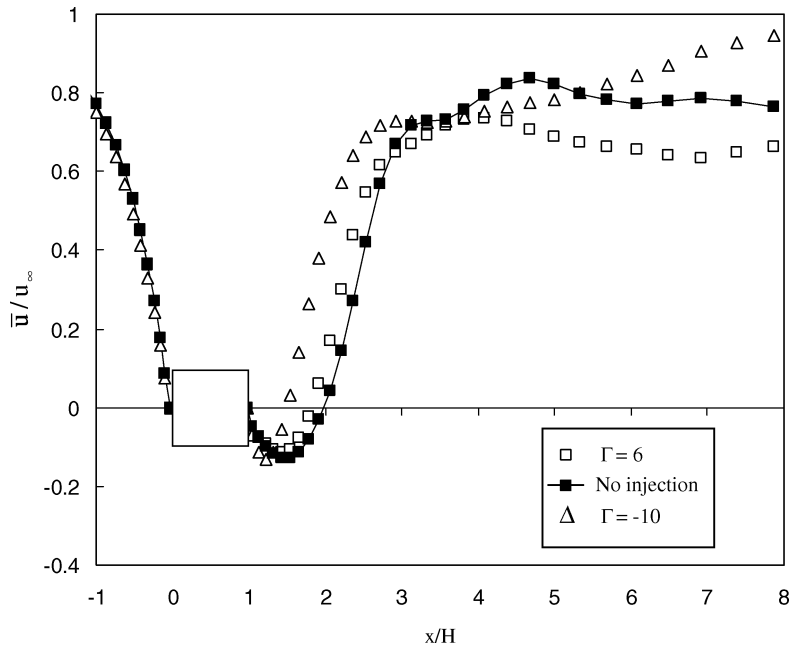


Figure 12.
 \bar{u}/u_∞ on the centre-line of the cylinder for the injection or suction through top and bottom surfaces

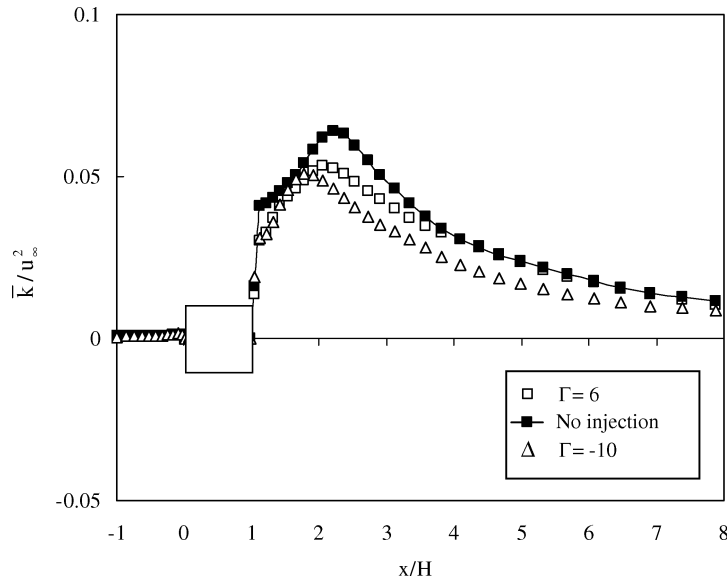


Figure 13.
 \bar{k}/u_∞^2 on the centre-line of the cylinder for the injection or suction through top and bottom surfaces

4.5 Injection or suction through all surfaces

This configuration can be regarded as the superposition of the one-surface injection or suction applications. The increasing injection velocity through top-bottom and front surfaces contribute to increase of the $\overline{C_D}$, while the increasing injection velocity through rear surface contribute to decrease of the $\overline{C_D}$. For the case of suction through all surfaces, the suction through rear surface becomes dominant (Table VII). The highest values of the St were obtained for the high injection velocities of this configuration.

It is seen from Figures 14 and 15 that the increasing injection velocity enlarges the vortex formation length and the increasing suction velocity reduces it again. The

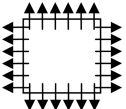
Configuration	Application	Γ	$\overline{C_D}$	C'_D	$\overline{C_L}$	C'_L	St
	Injection	6	2.3411	0.0381	0.0025	0.6988	0.1587
		5	2.3569	0.0306	0.0153	0.8676	0.1587
		4	2.3263	0.0183	-0.0003	0.9542	0.1587
		3	2.2753	0.0103	-0.0083	1.0074	0.1465
		2	2.1971	0.0104	-0.0021	1.0190	0.1465
		1	2.1417	0.0229	-0.0321	1.1418	0.1343
		No injection	0	2.1154	0.0470	0.0054	1.3837
	Suction	-1	2.1186	0.0842	0.0441	1.6109	0.1221
		-2	2.1109	0.1195	0.0097	1.7338	0.1221
		-3	2.1507	0.1663	0.0785	1.7843	0.1221
-4		2.5535	0.9424	0.1602	1.7206	0.1221	
-5		4.5203	0.8217	0.2806	2.1615	0.1099	
-6		4.6541	0.6862	0.2278	2.2051	0.1099	
-7		2.7300	0.2872	0.9644	1.2424	0.2075	

Table VII.
Results for injection and suction through all surfaces

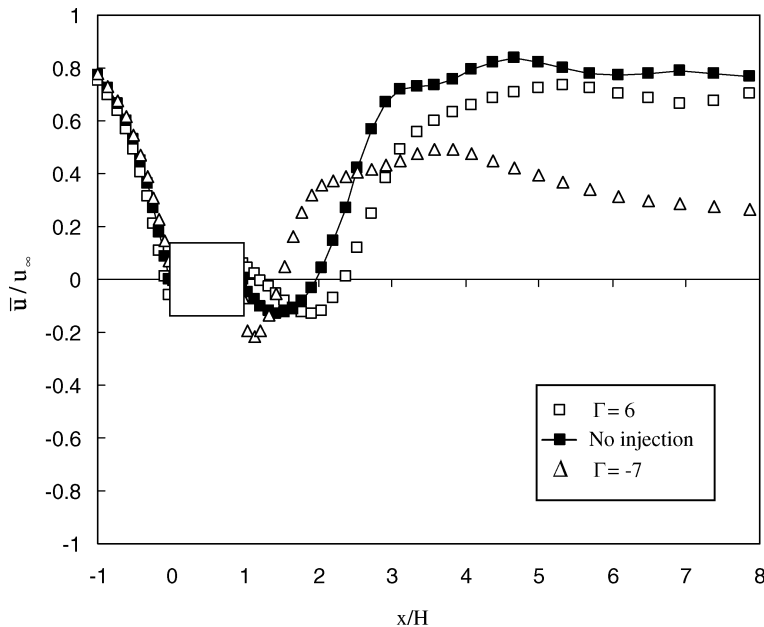


Figure 14.
 \bar{u}/u_∞ on the centre-line of the cylinder for the injection or suction through all surfaces

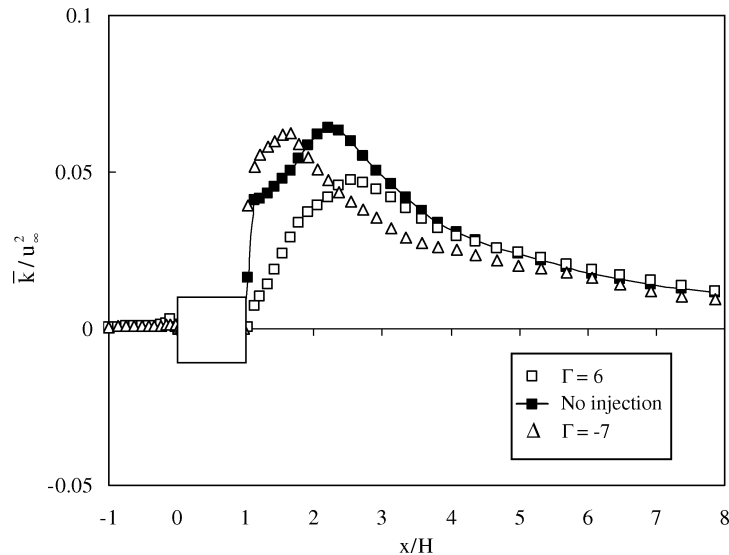


Figure 15.
 \bar{k}/u_∞^2 on the centre-line of the cylinder for the injection or suction through all surfaces

suction with $\Gamma = -7$ drastically reduces the \bar{u}/u_∞ values beyond the recirculation zone compared to the no-injection case.

5. Conclusions

The flow around a porous square cylinder with uniform injection and suction has been studied numerically. The injection and suction have been simulated using the WFs including injection and suction effects. The effects of injection or suction velocity and surface on the aerodynamic parameters of drag and lift coefficients and vortex-shedding frequency have been analyzed. Although the magnitude of injection and suction velocity is relatively lower than that of the main flow, it significantly changes drag and lift coefficients as well as vortex-shedding frequency.

The numerical results have shown that increasing suction velocity decreases the drag coefficient for all the suction configurations considered in the present study, except that of suction through rear surface. The lift coefficient substantially decreases with increasing velocity of suction through top surface. In addition, the vortex-shedding frequency is affected by injection and suction. The vortex-shedding motion gets weak by the suction application through top and bottom surfaces. Thus, it can be concluded that the injection and suction application through certain surfaces of a porous square cylinder can be regarded as a drag and wake control method. The heat transfer characteristics of the present study will also be analyzed in which the heat transfers between porous square cylinder with injection–suction and main flow.

References

- Bellettre, J., Bataille, F. and Lallemand, A. (1999), "A new approach for the study of turbulent boundary layers with blowing", *International Journal of Heat and Mass Transfer*, Vol. 42, pp. 2905-20.
- Bosch, G. and Rodi, W. (1998), "Simulation of vortex shedding past a square cylinder with different turbulence models", *International Journal for Numerical Methods in Fluids*, Vol. 28, pp. 601-16.

- Cadafalch, J., Perez-Segarra, C.D., Cònsul, R. and Oliva, A. (2002), "Verification of finite volume computations on steady-state fluid flow and heat transfer", *ASME Journal of Fluids Engineering*, Vol. 124, pp. 11-21.
- Çuhadaroğlu, B. (2004), "Numerical study of turbulent boundary layers with heat transfer and tangential transpiration", *International Journal of Numerical Methods for Heat and Fluid Flow*, Vol. 14 No. 6, pp. 760-82.
- Franke, R. and Rodi, W. (1991), "Calculation of vortex shedding past a square cylinder with various turbulence models", *Proceedings of the Eighth Symposium on Turbulent Shear Flows, Technical University of Munich, Munich*, paper 20-1.
- Fransson, J.H.M., Konieczny, P. and Alfredsson, P.H. (2004), "Flow around a porous cylinder subject to continuous suction or blowing", *Journal of Fluids and Structures*, Vol. 19, pp. 1031-48.
- Gorla, R.S.R., Slaouti, A. and Takhar, H.S. (1997), "Mixed convection in non-Newtonian fluids along a vertical plate in porous media with surface mass transfer", *International Journal of Numerical Methods for Heat and Fluid Flow*, Vol. 7 No. 6, pp. 598-608.
- Hannemann, K. and Oertel, H. Jr (1989), "Numerical simulation of the absolutely and convectively unstable wake", *Journal of Fluid Mechanics*, Vol. 199, pp. 55-88.
- Hirt, C.W. and Cook, J.L. (1972), "Calculating three-dimensional flows around structures and over rough terrain", *Journal of Computational Physics*, Vol. 10, pp. 324-40.
- Jue, T.-C. (2004), "Numerical analysis of vortex shedding behind a porous square cylinder", *International Journal of Numerical Methods for Heat and Fluid Flow*, Vol. 14 No. 5, pp. 649-63.
- Kato, M. and Launder B.E. (1993), "The modeling of turbulent flow around stationary and vibrating square cylinders", *Proceedings of the Ninth Symposium on Turbulent Shear Flows, Kyoto, August*, pp. 10.4.1-10.4.6.
- Lyn, D.A., Einav, S., Rodi, W. and Park, J.H. (1995), "A laser-doppler velocimetry study of ensemble-averaged characteristics of the turbulent near wake of a square cylinder", *Journal of Fluid Mechanics*, Vol. 304, pp. 285-319.
- Mathelin, L., Bataille, F. and Lallemand, A. (2002), "The effect of uniform blowing on the flow past a circular cylinder", *ASME Journal of Fluids Engineering*, Vol. 124, pp. 452-64.
- Meinert, J., Huhn, J., Serbest, E. and Haidn, O.J. (2001), "Turbulent boundary layers with foreign gas transpiration", *Journal of Spacecraft Rockets*, Vol. 38, pp. 191-8.
- Roache, P.J. (1997), "Quantification of uncertainty in computational fluid dynamics", *Annual Review of Fluid Mechanics*, Vol. 29, pp. 123-60.
- Schetz, J.A. and Nerney, B. (1977), "Turbulent boundary layer with injection and surface roughness", *AIAA Journal*, Vol. 15, pp. 1288-93.
- Schumm, M., Berger, E., and Monkewitz, P. (1994), "Self-excited oscillations in the wake of two-dimensional bluff bodies and their control", *Journal of Fluid Mechanics*, Vol. 271, pp. 17-53.
- White, F.M. (1999), *Fluid Mechanics*, McGraw-Hill, New York, NY.

Corresponding author

Burhan Çuhadaroğlu can be contacted at: burhan@ktu.edu.tr